



## Early assessment of Integrated Multi-satellite Retrievals for Global Precipitation Measurement over China

Hao Guo <sup>a,b</sup>, Sheng Chen <sup>c,d,\*</sup>, Anming Bao <sup>a</sup>, Ali Behrangi <sup>e</sup>, Yang Hong <sup>d</sup>, Felix Ndayisaba <sup>a,b</sup>, Junjun Hu <sup>f</sup>, Phillip M. Stepanian <sup>g</sup>

<sup>a</sup> State Key Laboratory of Desert and Oasis Ecology, Xinjiang Institute of Ecology and Geography, Chinese Academy of Sciences, Urumqi 830011, China

<sup>b</sup> University of Chinese Academy of Sciences, Beijing 100049, China

<sup>c</sup> School of Atmospheric Sciences, Sun Yat-sen University, Guangzhou 510275, China

<sup>d</sup> School of Civil Engineering and Environmental Science, University of Oklahoma, Norman, OK 73072, USA

<sup>e</sup> Jet Propulsion Laboratories, California Institute of Technology, Pasadena, CA 91109, USA

<sup>f</sup> School of Computer Science, University of Oklahoma, Norman, OK 73072, USA

<sup>g</sup> School of Meteorology, Advanced Radar Research Center, University of Oklahoma, Norman, OK, USA



### ARTICLE INFO

#### Article history:

Received 26 November 2015

Received in revised form 25 January 2016

Accepted 22 February 2016

Available online 27 February 2016

#### Keywords:

Global Precipitation Measurement

Remote sensing

Satellite

Precipitation

### ABSTRACT

Two post-real time precipitation products from the Integrated Multi-satellite Retrievals for Global Precipitation Measurement Mission (IMERG) are systematically evaluated over China with China daily Precipitation Analysis Product (CPAP) as reference. The IMERG products include the gauge-corrected IMERG product (IMERG\_Cal) and the version of IMERG without direct gauge correction (IMERG\_Uncal). The post-research TRMM Multisatellite Precipitation Analysis version 7 (TMPA-3B42V7) is also evaluated concurrently with IMERG for better perspective. In order to be consistent with CPAP, the evaluation and comparison of selected products are performed at 0.25° and daily resolutions from 12 March 2014 through 28 February 2015.

The results show that: Both IMERG and 3B42V7 show similar performances. Compared to IMERG\_Uncal, IMERG\_Cal shows significant improvement in overall and conditional bias and in the correlation coefficient. Both IMERG\_Cal and IMERG\_Uncal perform relatively poor in winter and over-detect slight precipitation events in northwestern China. As an early validation of the GPM-era IMERG products that inherit the TRMM-era global satellite precipitation products, these findings will provide useful feedbacks and insights for algorithm developers and data users over China and beyond.

© 2016 Elsevier B.V. All rights reserved.

### 1. Introduction

Precipitation measurements provide essential information for various applications such as numerical weather prediction, climate modelling, global energy and circulation pattern analysis, and climate diagnostic studies (Arkin & Xie, 1994; Kidd et al., 2012). Such data are critical sources of the main inputs to hydrologic, climatologic, and agricultural studies (Chen et al., 2013b; Habib et al., 2012; Seyyedi et al., 2015; Tang et al., 2015). Despite their great importance for different applications, reliable and accurate measurements of precipitation at global or regional scales with high resolution remain a scientific challenge because of the great heterogeneity across different spatiotemporal applications (Chen et al., 2013a; Li et al., 2013; Lo Conti et al., 2014; Mei

et al., 2014). Common approaches for quantifying precipitation include ground rain gauge observations, weather radars, and estimates from satellite observations. Conventional rain gauge networks provide a direct physical measurement of surface precipitation amount with high temporal frequency (Xie & Arkin, 1995, 1996). However, the inhomogeneous distribution of rain gauges, limited spatial representativeness, and data latency hamper the use of these data for some applications (Ebert et al., 2007; Kidd et al., 2012; Porcù et al., 2014). Ground-based weather radars can provide precipitation estimates with relatively high spatial and temporal resolutions, but with limited coverage, variable accuracy, and limited utility in cold weather and mountainous terrain (Anagnostou, 2004; Ciach et al., 2007; Germann et al., 2006; Mei et al., 2014; Piccolo & Chirico, 2005; Schneebeli et al., 2013; Sharif et al., 2002). Precipitation estimates from satellite-based sensors may have great potential for various applications due to their extensive spatial coverage, consistent measurements over land and oceanic regions, as well as free access to near real-time data through the Internet (Bajracharya et al., 2015; Barrera et al., 2007; Karaseva et al., 2012; Stisen & Sandholt, 2010). Some of them have fine spatial and temporal resolutions and can provide information on precipitation occurrence,

\* Corresponding author at: School of Atmospheric Sciences, Sun Yat-sen University, Guangzhou 510275, China. Tel./fax: +86 20 8411 1286.

E-mail addresses: casguohao@163.com (H. Guo), chenshengbj@gmail.com (S. Chen), baoam@ms.xjlab.ac.cn (A. Bao), ali.behrangi@jpl.nasa.gov (A. Behrangi), yanghong@ou.edu (Y. Hong), dafelix@yahoo.fr (F. Ndayisaba), junjun.Hu-1@ou.edu (J. Hu), step@ou.edu (P.M. Stepanian).

amount and distribution with smaller errors in area averaged estimation over sub-basins, even when precipitation at a single pixel may be not precise (Barrera et al., 2007).

Since the launch of the Tropical Rainfall Measuring Mission (TRMM) in 1997, extensive efforts have been made in developing satellite-based quantitative precipitation estimates (QPE) algorithms and operational satellite-based QPE products with high resolution. A series of TRMM-era satellite-based precipitation retrieval algorithms have been generated through the combined use of infrared (IR) and passive microwave (PMW) observations from multiple satellite sensors, such as TRMM Multi-satellite Precipitation Analysis (TMPA) (Huffman et al., 2007), Climate Prediction Center morphing technique (CMORPH) (Joyce et al., 2004), Precipitation Estimation from Remotely Sensed Information using Artificial Neural Networks (PERSIANN) (Hong et al., 2004; Hsu et al., 1997; Sorooshian et al., 2000), and Global Satellite Mapping of Precipitation (GSMap) (Kubota et al., 2007; Okamoto et al., 2005). The ongoing efforts to improve retrieval algorithms and estimation techniques from the scientific community have resulted in the start of the GPM era.

The Global Precipitation Measurement (GPM) mission is composed of an international network of satellites that provide the next-generation global observations of rain and snow. As a global successor to TRMM, GPM focuses on the deployment of a "Core" satellite carrying an advanced radar/radiometer system to measure precipitation from space and serve as a reference standard to unify precipitation measurements from a constellation of research and operational satellites. The post-real time product Integrated Multi-satellite Retrievals for GPM (IMERG) is now available online at <https://stommpp.gsfc.nasa.gov/storm>. Much effort has been made to investigate the error and uncertainty characteristics of satellite-based precipitation products, such as TRMM, GSMap, CMORPH, and PERSIANN over China (Chen et al., 2013b; Chen et al., 2014; Chen et al., 2016; Gao & Liu, 2013; Guo et al., 2015a; Liu et al., 2014; Qin et al., 2014; Shen et al., 2010b; Yin et al., 2008; Zhou et al., 2008). However, there have been very few reports associated with verification of IMERG products. Here we evaluate the performance of IMERG (latest released version) over China. This is one early study to assess the performance of the post-research product of IMERG with and without calibration over China, spanning the time from 12 March 2014 through 28 February 2015. Specifically, the error structures analyzed are characterized in terms of spatial distribution, temporal variation, and frequency of precipitation with different intensities. To obtain a better perspective of the error characteristics associated with the IMERG products, the version 7 post research product of TRMM Multisatellite Precipitation Analysis (TMPA) (hereafter, 3B42V7) is also included in this evaluation. 3B42V7 has been extensively evaluated in previous studies (Casse et al., 2015; Chen et al., 2013b; Chen et al., 2013c; Gao & Liu, 2013; Ghajarnia et al., 2015; Guo et al., 2015b; Huang et al., 2013; Liu, 2015; Shen et al., 2010b) and the strengths and weaknesses of the product are well understood. Building upon extensive existing studies on satellite-based precipitation products in the TRMM era, the goal of this study is to yield more insight into IMERG's error characteristics, thus providing useful information for users of the IMERG products and developers of IMERG algorithms.

The rest of this paper is organized as follows. Section 2 introduces the study region, the IMERG products, ground reference dataset, and evaluation metrics. Section 3 focuses on the analysis of spatial characteristics and the error quantification for IMERG. A brief summary and conclusions are given in Section 4.

## 2. Study region and datasets

### 2.1. Study region

The geography of China is variable, with regional differences in topography. A map showing the topographic variability from a digital elevation model (DEM) is given in Fig. 1a. Similar to the divisions

presented in Chen et al. (2013b), China is separated into seven subregions in terms of elevation, mountain ranges (Tang et al., 2006) and the annual mean precipitation distribution (Qian & Lin, 2005). These subregions are shown in Fig. 1a and are referred to as: I) the Xinjiang (XJ) region, which has arid and semi-arid climate characteristics; II) Qinghai-Tibet Plateau (TP) which has an average elevation about 4500 m; III) Northwestern China (NW) bounded by the 400 mm annual precipitation isohyet; IV) Northeastern China (NE) located in the north of Yan mountain; V) Northern China (NC) located in the north of Qinling Mountains-Huai River line; VI) Yunnan-Guizhou Plateau in southwestern China (SW) which is bounded by the Ta-pa Mountains and Wulingshan mountains to the north and east; and VII) Southern China (SC) south of the Nanling mountains and southeast of the Wuyi Mountains. These subregion abbreviations are labeled in Fig. 1a, and will be used herein.

The climate in XJ is characterized by semi-arid climates, and its precipitation is primarily influenced by the mid-latitude westerlies with moisture contributions from the North Atlantic Ocean (Bothe et al., 2012). Coupled with the effects of complex terrain, the East Asia subtropical monsoon brings a large amount of precipitation over eastern China. The rainy season in most of China generally begins with the onset of the summer monsoon and ends with its withdrawal (Zhou et al., 2009). The monsoon rain belt moves from low latitudes to mid-high latitudes as the summer monsoon advances northward (Liu & Wang, 2011). The shift of the monsoon (Shen et al., 2010b; Zhou et al., 2008) and the landfall of typhoons (Carr & Elsberry, 1995) result in the Mei-yu, a persistent front of convective rainfall, from June and July in along the Yangtze-Huai river valley. Southwestern China is dominated by the monsoon between the Qinghai-Tibet Plateau (TP) and the Indian Ocean.

### 2.2. Ground reference dataset

The China daily Precipitation Analysis Product (CPAP) is produced and routinely calibrated by the National Meteorological Information Center (NMIC) and China Meteorological Administration (CMA). The CPAP product with a 0.25°/daily spatiotemporal resolution is used as a reference to evaluate the IMERG precipitation products. About 2400 heated rain gauge observations were interpolated with the climatology-based Optimal Interpolation (OI) technique to yield the gridded analysis product. Snowfall can be measured accurately by these heated rain gauges through manual heating method (Yan Shen, personal communication, January, 2016). An objective technique was used to define CPAP (Chen et al., 2008; Xie & Xiong, 2011; Xie et al., 2007), and the Parameter-Elevation Regression on Independent Slopes Model (PRISM) is used to correct orographic errors (Chen et al., 2016). All the gauge data used in CPAP have undergone strict quality control in three levels including the extreme values' check, internal consistency check, and spatial consistency check (Shen et al., 2010b). CPAP has been systematically validated by Shen (Shen & Xiong, 2015), and found that the daily analysis has very good agreements with the observations over different regions of China (Shen & Xiong, 2015). CPAP exhibits a relative bias of 3.21% at the 0.5° scale when compared to independent gauge observations in the validation (Shen et al., 2010a). And the gauge-based dataset has been successfully adopted to validate high resolution satellite-based precipitation estimates by some studies (Chen et al., 2013b; Chen et al., 2016; Guo et al., 2015a; Qin et al., 2014; Shen et al., 2010b).

The spatial distribution of rain gauge locations in Fig. 1b used in this study for a typical day represents the median gauge number for the whole study period. The Chinese rain gauge network is distributed unevenly over China. Gauge stations are densely spaced in eastern China where it is climatically wet and the population is dense, whereas relatively sparse gauge stations are found in western China. Gauges are especially infrequent in the areas of NW, XJ and TP, all of which are dominated by semiarid and arid climates. The limited number could

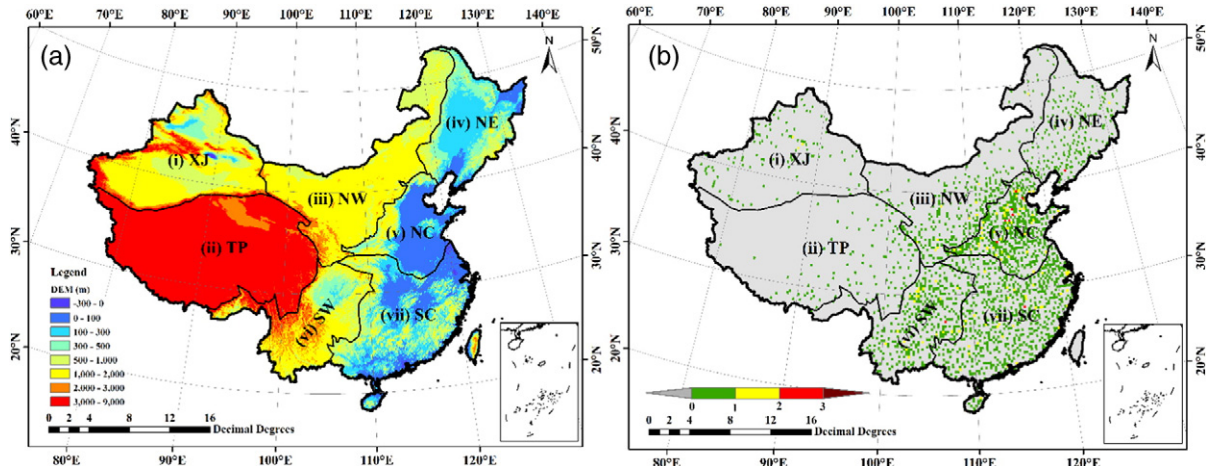


**Fig. 1.** (a) Topographic feature in China. The black solid line indicates the outline of the seven subregions: (i) Xinjiang (XJ), (ii) Qinghai-Tibetan plateau (TP), (iii) Northwest (NW), (iv) Northeast (NE), (v) North (NC), (vi) southwest Yungui Plateau (SW), and (vii) South (SC). (b) A  $0.25^\circ \times 0.25^\circ$  density map of gauges over China with about 2400 gauges used in CPAP. The white panel in the lower right corner of each figure represents the South China Sea region. China's borders were downloaded from National Administration of Surveying, Mapping, and Geoinformation with No. GS(2008)1045.

be a source of error in evaluation of these selected products (Shen et al., 2014). It is worth mentioning that the gauges used in CPAP are not completely independent of those used in IMERG\_Cal and 3B42V7, since ~500 out of the total gauges (~2400) from CPAP are potentially applied in the GPCC dataset that is used to correct IMERG\_Cal and 3B42V7. The assessment results may be influenced to some extent by the location of coincident gauges, especially for western China (e.g. TP, XJ and NW) with sparse rain gauges.

### 2.3. Satellite-based precipitation dataset

The calibrated and uncalibrated IMERG datasets are obtained using the Day-1 U.S. multi-satellite algorithm for GPM (Huffman et al., 2014). IMERG has been developed as a unified U.S. algorithm drawing on strengths from three prior multi-satellite algorithms from NASA (i.e. TRMM Multi-satellite Precipitation Analysis; TMPA (Huffman et al., 2007)), National Oceanic and Atmospheric Administration (NOAA; CPC Morphing-Kalman Filter; CMORPH-KF (Joyce & Xie, 2011)), and University of California Irvine (Precipitation Estimation from Remotely Sensed Information using Artificial Neural Networks-Cloud Classification System; PERSIANN-CCS (Hong et al., 2004)). Passive microwave (PMW) sensors, carried by satellites in low earth orbits (LEO), provide relatively accurate satellite-based precipitation estimates by directly sensing rainfall, but offer quite limited samples. IR sensors can provide excellent temporal resolution of top temperatures from geosynchronous orbit (GEO) satellites, but the indirect relationship with precipitation results in great uncertainty (Hsu & Sorooshian, 2008; Karaseva et al., 2012). In order to compensate for the limited sampling available from single LEO satellites, IMERG is designed to use as many PMW estimates as possible and fill in gaps with GEO IR estimates. The PMW estimates are gridded, intercalibrated, and morphed, following the GEO-IR-based feature motion. When the LEO-PMW estimates are too sparse, the GEO-IR precipitation estimates from PERSIANN-CCS are integrated. Precipitation gauge analyses are induced to provide crucial regionalization and bias-correction to the satellite estimates. More detailed information regarding IMERG can be obtained from "IMERG Algorithm Theoretical Basis Document" available online at [http://pmm.nasa.gov/sites/default/files/document\\_files/IMERG\\_ATBD\\_V4.4.pdf](http://pmm.nasa.gov/sites/default/files/document_files/IMERG_ATBD_V4.4.pdf) and the technical document accessible at [http://pmm.nasa.gov/sites/default/files/document\\_files/IMERG\\_doc.pdf](http://pmm.nasa.gov/sites/default/files/document_files/IMERG_doc.pdf).

IMERG provides three types of products: early run, late run, and final run products. Both the early run and late run products are near-real-time, with a latency of 4 h and 12 h, respectively. The final run product

is a post-real-time research product that is available from 12 March 2014 with a latency of about 4 months. Both the half-hourly and monthly IMERG final run products are released at the same  $0.1^\circ \times 0.1^\circ$  spatial resolution. The half-hourly product (latest released version) was selected for evaluation in this study from 12 March 2014 to 28 February 2015 over China. Unless otherwise indicated, the abbreviation IMERG refers to the final run product of IMERG in the following sections for simplicity. Both the uncalibrated and calibrated multi-satellite precipitation information (hereafter referred to as IMERG\_Uncal and IMERG\_Cal) are provided in IMERG final run. In contrast to IMERG\_Uncal, a monthly gauge dataset (i.e. the monitoring product) from the Global Precipitation Climatology Centre (GPCC) is introduced into the bias-correction algorithm for IMERG\_Cal. Gauge adjustment has been shown as an effective enhancement to satellite products (Chen et al., 2013b; Chen et al., 2013c). In order to keep consistent with the ground reference dataset, both IMERG\_Uncal and IMERG\_Cal with native  $0.1^\circ$ /hourly spatiotemporal resolution are aggregated into 0.25-degree spatial and daily temporal resolutions. However, readers should keep in mind that regridding the products might introduce additional uncertainties.

The TMPA algorithm was developed by the National Aeronautics and Space Administration (NASA) Goddard Space Flight Center (GSFC) (Huffman et al., 2007). The TMPA combines two interim products: PMW data and PMW calibrated IR. The PMW data are calibrated by the combined TMI and precipitation radar (PR) products, and then used to calibrate the IR input data. Version 7 of TMPA includes two types of products: The real-time version (3B42RTV7) covering the global latitude belt from  $60^\circ\text{N}$  to  $60^\circ\text{S}$ , and the gauge-adjusted, post-real-time research product (3B42V7) with the coverage of the latitude belt from  $50^\circ\text{N}$  to  $50^\circ\text{S}$ . As a similar post-research precipitation product, the post-real-time research product (3B42V7) with  $0.25^\circ$ -daily spatiotemporal resolution is evaluated in parallel with the IMERG products. Three products are employed to generate 3B42V7, including the TRMM Combined Instrument (TCI) estimate, the Global Precipitation Climatology Center (GPCC)  $1^\circ$  monthly gauge product, and the Climate Assessment and Monitoring System (CAMS, V6 only)  $0.5^\circ \times 0.5^\circ$  monthly gauge data.

### 2.4. Statistics evaluation metrics

A series of traditional error indexes, which include Bias, Relative Bias (RB), Root Mean Square Error (RMSE), Pearson linear Correlation Coefficient (CC) and Fractional Standard Error (FSE), are introduced in this study. RB, FSE and CC are dimensionless, and RMSE is in mm/day. RB,

when multiplied by 100, denotes the degree of overestimation or underestimation in percentage. The definition of RB, CC, and RMSE can be found in Chen et al. (2013c), and FSE is defined as follows:

$$FSE = \sqrt{\frac{\frac{1}{N} \sum_{i=1}^N (S_i - G_i)^2}{\frac{1}{N} \sum_{i=1}^N G_i}} \quad (1)$$

where N is the number of samples, and S and G are the satellite-based products and the reference dataset, respectively.

To evaluate precipitation detection capabilities of IMERG and 3B42V7 by taking CPAP precipitation detection as a reference, three categorical statistical indices including Probability of Detection (POD), False Alarm Ratio (FAR), and Equitable Threat Score (ETS) also are calculated based on construction of a contingency table (Nurmi, 2003). POD represents the ratio of the correct identification of rainfall by satellite-based precipitation products to the number of rainfall occurrences observed by the reference; FAR denotes the proportion of cases in which the satellite-based precipitation products record rainfall when the rain gauges do not; and ETS is a measure of the overall accuracy of rainfall

events correctly diagnosed by the satellite with random chance. POD, FAR and ETS range from 0 to 1, with 1 being a perfect POD and ETS, while 0 is a perfect FAR. All above statistics have been computed on a grid-by-grid basis over China. Taylor diagrams are also included to visualize and quantify the overall performance of various products. The definition of the Taylor diagram can be found in Taylor (2001).

### 3. Result analysis and discussion

#### 3.1. One year precipitation analysis

As shown in Fig. 2, the mean precipitation over the southern part of China (i.e. SW and SC) is much higher than that over northern China (i.e. XJ, TP, NW, NE and NC). Both IMERG\_Cal and 3B42V7 perform well in capturing the spatial patterns of precipitation over China, except for a slight underestimation of precipitation over the valley in western Tianshan Mountain, located in the western part of XJ. However, subtle differences still exist between the two, with IMERG\_Cal having smoother rain patterns. In contrast, IMERG\_Uncal (Fig. 2c) tends to underestimate the rainfall over the SW, SC and TP regions, and overestimates the precipitation over the NW and NE regions.

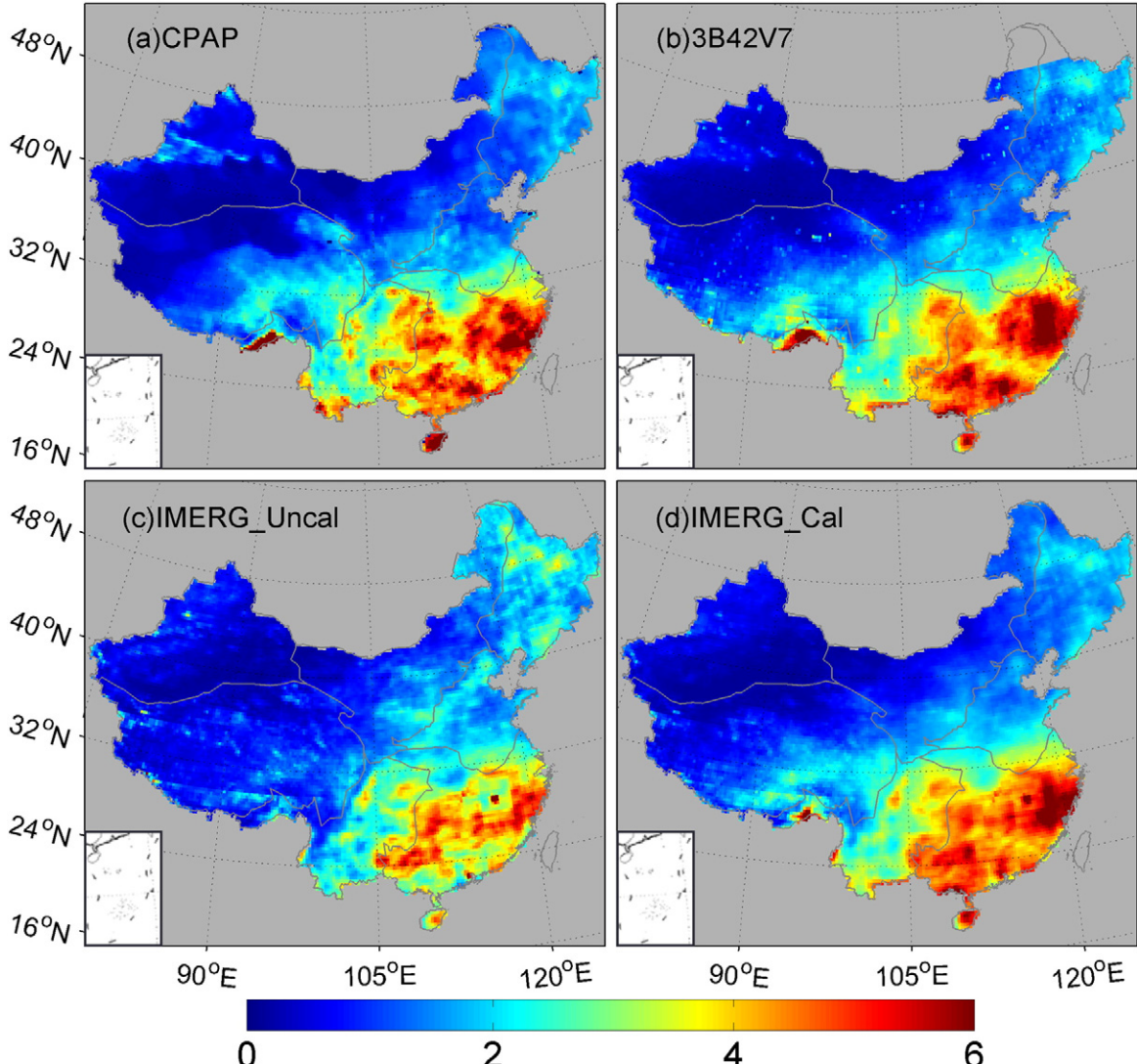


**Fig. 2.** Spatial distribution of near one-year mean precipitation ranging from 12 March 2014 to 28 February 2015 derived from (a) CPAP, (b) 3B42V7, (c) IMERG\_Uncal, and (d) IMERG\_Cal over China. The white panel in the lower left corner of each figure represents the South China Sea region.

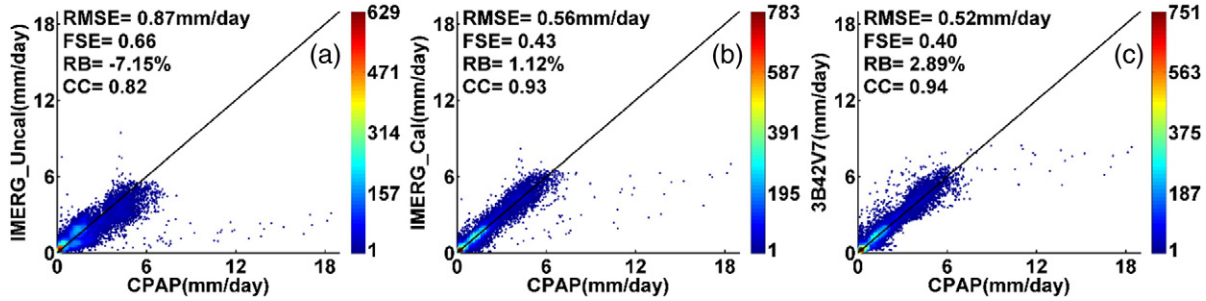


**Fig. 3.** Density-colored scatterplots of three products against CPAP rainfall rate for (a) IMERG\_Uncal, (b) IMERG\_Cal, and (c) 3B42V7 over China. The color represents the occurrence frequency. The dark oblique solid line denotes 1:1 line.

**Fig. 3** shows the density-colored scatterplots of the IMERG products and 3B42V7 versus the CPAP product for the quantitative comparison of mean daily precipitation over the entire mainland China throughout the

full study period. The density-colored scatter plots and corresponding error statistics reveal that IMERG\_Cal exhibits a comparable performance with 3B42V7. Both IMERG\_Cal and 3B42V7 have high CC (0.93

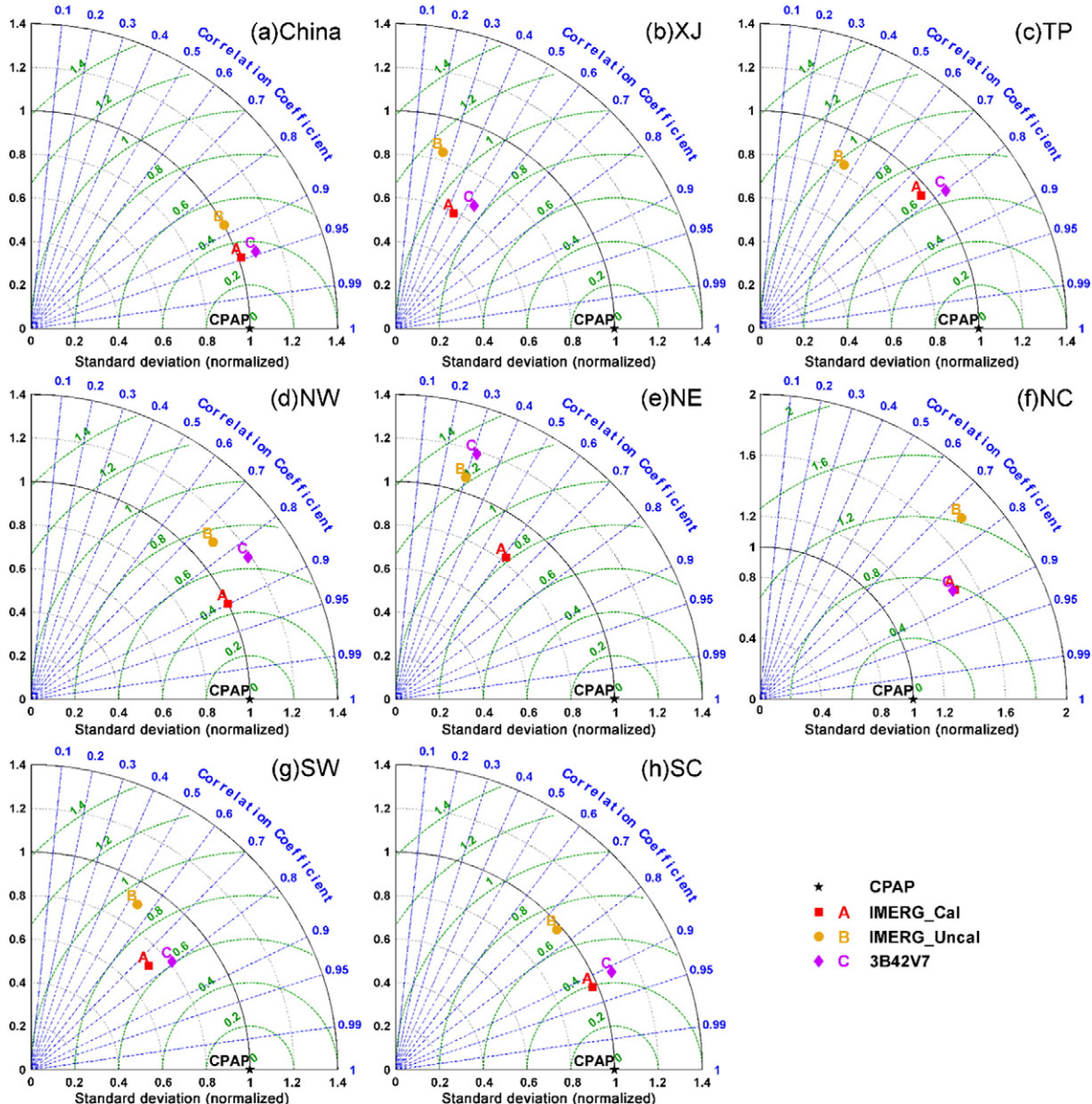


**Fig. 4.** Taylor diagrams showing correlation coefficients, standard deviation (normalized), and RMSE of four year daily mean precipitation between the satellite-based precipitation products and the reference data over (a) mainland China, and seven subregions, (b) XJ, (c) TP, (d) NW, (e) NE, (f) NC, (g) SW, and (h) SC.

and 0.94, respectively), and low RB (1.12% and 2.89%, respectively), RMSE (0.56 and 0.52 mm/day, respectively) and FSE (0.43 and 0.40, respectively). Without the monthly gauge-correction, IMERG\_Uncal tends to underestimate precipitation with the highest RB (−7.15%), RMSE (0.87 mm/day) and FSE (0.66), and the lowest CC (0.82).

In addition to the statistics over mainland China, RB, RMSE, FSE and CC are given in [Appendix A](#) over seven subregions. IMERG\_Cal gives a similar performance with 3B42V7 and improves the overestimation or underestimation of IMERG\_Uncal, generally with much smaller magnitudes according to the corresponding CC, RB, RMSE and FSE values ([Appendix A](#)). This improvement is particularly evident in TP, NW, NE, SW, and SC in terms of RB, RMSE and FSE. Specifically, IMERG\_Uncal shows a significant underestimation of precipitation over TP, SW, and SC subregions with negative RBs (−26.70%, −28.34% and −14.99%, respectively) and a numerically fluctuating overestimation over NW, NE, and NC with positive RBs (34.47%, 30.42% and 15.21%, respectively). This result is consistent with the spatial pattern of summer mean precipitation shown in [Fig. 2c](#). The great underestimation over TP may be attributed, at least partially, to the complicated terrain and sparse distributed gauges stations, as well as OI interpolation. A possible explanation of the overestimation over NE may be caused by the poor snowfall estimates over the long winter season in these high-latitude regions.

Interestingly, both IMERG\_Cal and 3B42V7 underestimate precipitation significantly (RB, −26.84% and −31.55%, respectively) over XJ, while IMERG\_Uncal without direct gauge adjustment displays relatively low RB (−6.21%) but relatively low CC (0.51). The considerable underestimation for IMERG\_Cal and 3B42V7 may be related to the sparse unevenly spaced gauge stations and the OI interpolation technique. Additionally, the abundance of topographically driven precipitation and fewer favorable land surface conditions (e.g. deserts, mountains, snow and ice cover) should be considered because both passive microwave and IR satellites have difficulty detecting shallow orographic precipitation ([Adeyewa & Nakamura, 2003; Karaseva et al., 2012; Taniguchi et al., 2013](#)).

In order to determine which product more precisely estimates precipitation over mainland China and seven subregions, Taylor diagrams ([Fig. 4](#)) proposed by Taylor (2001) are plotted to visualize the concise statistical summary of how well patterns match between various products and reference data (CPAP) over China and seven subregions in terms of their correlation coefficient, the ratio of their standard deviation and their RMSE values. The radial coordinate in Taylor Diagrams is the magnitude of standard deviation, which is normalized by the standard deviation from CPAP and denoted by black dotted lines, and the concentric green semi-circles denote RMSE values. Meanwhile, the

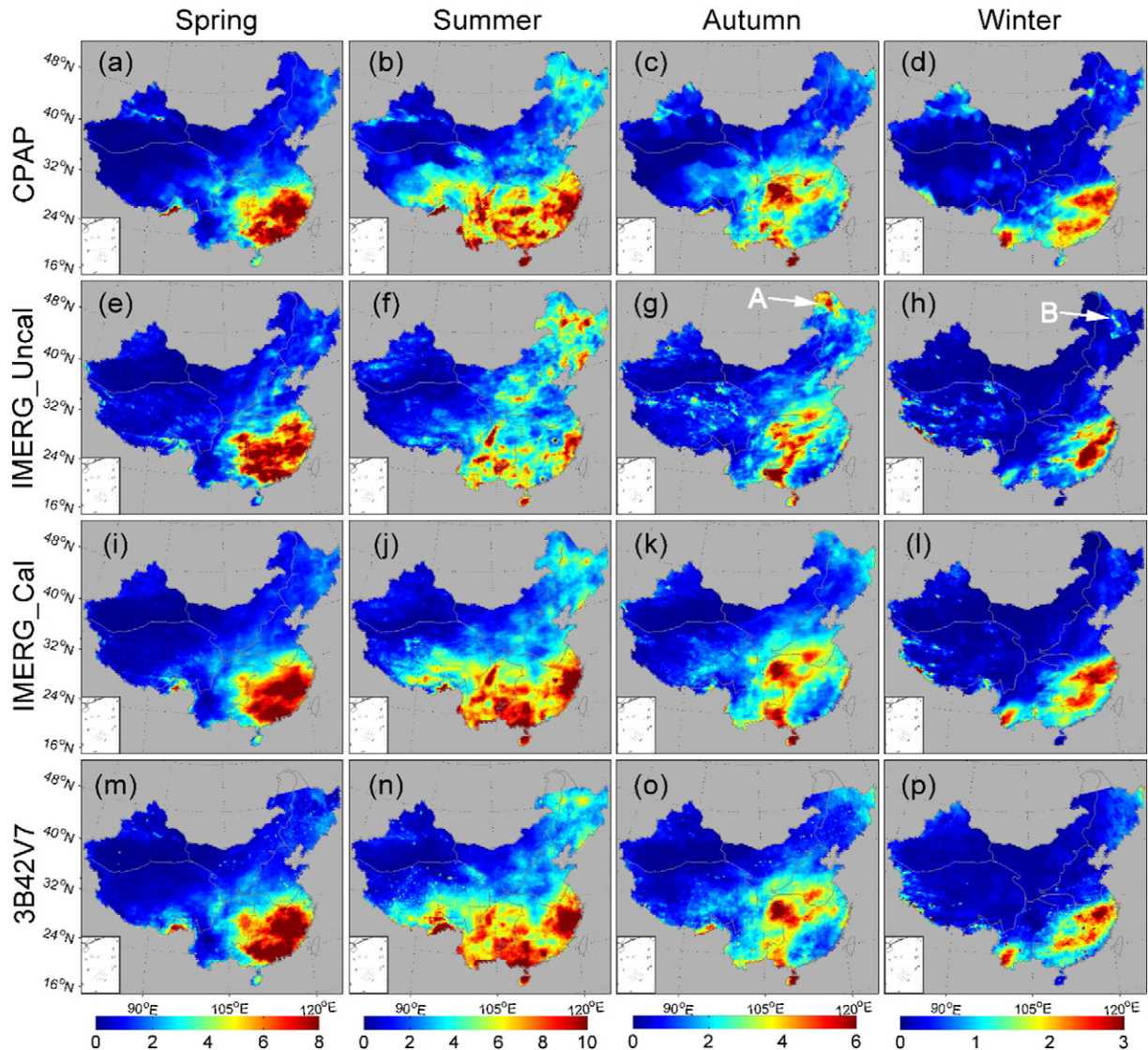


**Fig. 5.** Seasonal near one-year daily mean precipitation distributions over China for CPAP, IMERG\_Uncal, IMERG\_Cal and 3B42V7 (a–p).

angular coordinate shows the correlation coefficient (denoted by blue dotted lines). In these Taylor diagrams, the closer the points representing the satellite-based precipitation products are to the CPAP point marked by the black star, the better the product. As is shown in Fig. 4, the superiority of gauge-corrected IMERG\_Cal is clearly evident with much closer distance to CPAP than IMERG\_Uncal over mainland China and subregions. In comparison with 3B42V7, IMERG\_Cal shows a similar performance over China, TP, NC, XJ and SW and has particular better performance in NW and NE which may be, at least partially caused by snow or ice. However, IMERG\_Cal suffers from slightly lower STDs and CCs over XJ and SW with complicated terrain.

Generally, IMERG\_Cal gives a comparable performance with 3B42V7 and greatly improves the quality of IMERG\_Uncal in terms of the qualitative spatial distribution and quantitative error indexes (i.e. Bias, RB, RMSE and CC). The fact that IMERG\_Cal and 3B42V7 have the similar performances should not be a surprise, for at least two reasons: On one hand, they are corrected over the same rain gauges; on the other hand, the first version of the DPR rain products (included in IMERG) is based on the TRMM-PR database.

### 3.2. Seasonal precipitation analysis

Precipitation over China varies dramatically, geographically and seasonally due to the influences of the Asian monsoon, the Tibetan plateau, and the baroclinic westerlies initiated from North Atlantic Ocean. Fig. 5 illustrates the seasonal mean precipitation patterns over China. For four seasons, all three products capture the general precipitation patterns over most parts of China. However, IMERG\_Uncal estimates less precipitation over SW and SC and overestimates precipitation over NE. In addition, abnormal overestimation patterns in IMERG\_Uncal can be seen over NE in autumn and winter (denoted by white letters A in Fig. 5g and B in Fig. 5h), which may be due to the snowfall over these high-latitude regions.

Seasonal performances of three satellite-based precipitation products are quantified in Fig. 6. The statistics of RB, RMSE and CC were computed from the corresponding seasonal mean precipitation accumulations shown in Fig. 5. Additionally, the statistics (RB, RMSE

and CC) over seven subregions are provided in Appendix A. It should be explicitly noted here that none of the three products is able to estimate highest rain rates, especially in spring and summer, when the highest values are measured by rain gauges. This is also evident in Fig. 3. IMERG\_Uncal shows a reasonable performance according to RBs (from  $-0.91\%$  in autumn to  $-23.60\%$  in winter), RMSEs (from 0.56 mm/day in winter to 2.30 mm/day in summer), FSEs (from 1.79 in winter to 1.26 in summer) and CCs (from 0.64 in winter to 0.88 in spring). After gauge calibration, IMERG\_Cal demonstrates a favorable performance in every season with high CCs (ranging from 0.84 in winter to 0.95 in spring), and small RBs (ranging from  $-12.68\%$  in winter to 0.21% in summer), FSEs (ranging from 0.46 in autumn to 0.78 in summer) and RMSEs (ranging from 0.36 mm/day in winter to 1.42 mm/day in summer). This indicates that the bias-correction procedure in IMERG\_Cal has greatly improved the quality of IMERG\_Uncal over China during this study period, according to RB, RMSE, FSE and CC. The performance of IMERG\_Cal is close to 3B42V7 in terms of CCs in spring (0.95 vs. 0.95), summer (0.88 vs. 0.90), autumn (0.91 vs. 0.91) and winter (0.84 vs. 0.83). In addition, IMERG\_Cal shows a slight superiority over 3B42V7 according to RBs in spring (6.92% vs. 10.54%) and summer (0.21% vs. 2.62%), but a slightly poorer performance in autumn (1.39% vs.  $-1.02\%$ ) and winter ( $-12.68\%$  vs.  $-9.07\%$ ). This may be related to the less-well capability of DPR algorithm quantifying solid (snowfall) precipitation. It is noted that all three satellite-based precipitation products display the poorest performance in winter with the highest RB values. IMERG\_Uncal significantly underestimates precipitation with RB up to  $-23.60\%$ , although this underestimation has been improved by direct gauge adjustment in IMERG\_Cal with RB about  $-12.68\%$ . Compared with the other three seasons, 3B42V7 also displays the largest RB ( $-9.07\%$ ) in winter. This underestimation may be influenced by the presence of a snow and ice covered surface in winter because the accuracy of PMW-based algorithms is influenced by snow and ice land cover (Tian et al., 2007), and specifically the PMW-based retrievals, e.g., AMSE-E, AMSU-B and SSM/I are degraded by the presence of snow cover (Ferraro et al., 1998; Grody, 1991).

On the regional scale, IMERG\_Uncal underestimates precipitation over TP, SW and SC in summer. The underestimation is as large as  $-52.29\%$  in

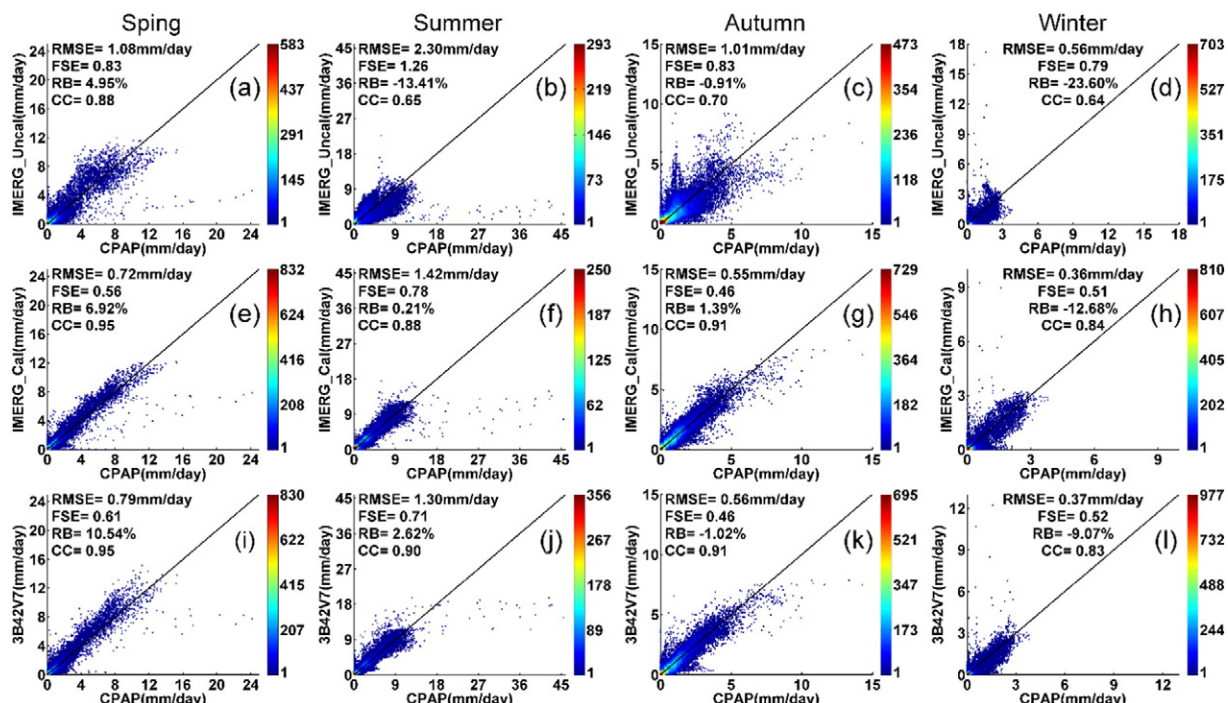


Fig. 6. Density-colored scatterplots of the IMERG products against CPAP rainfall rate shown in Fig. 5. The color represents the occurrence frequency (a–l).

TP, –30.34% in SW, and –30.68% in SC. This contribution can be partially responsible for the general underestimation over the mainland of China. IMERG\_Uncal also shows significant overestimation in summer over NW and NE, with positive RBs (58.51% and 44.70%). After the gauge correction is applied to IMERG\_Uncal (to create IMERG\_Cal), there is a reduction of RBs, RMSEs, and FSEs and a dramatic increase in CCs in various subregions. The performance of IMERG\_Cal is close to 3B42V7 in different subregions with similar CCs, RBs, RMSEs and FSEs.

### 3.3. Daily precipitation analysis

In order to investigate the temporal behavior of Bias, RMSE, and CC of IMERG\_Uncal and IMERG\_Cal over China, comparison statistics of

daily precipitation over China are provided for seven subregions during the whole study period (Fig. 7). It has been reported that a sparse observation network degrades the quality of gauge-based analysis (Xie et al., 2007) and additionally, a substantial magnitude of both bias and random errors may occur in the gauge-based analysis over grid boxes with no gauge reports available nearby (Chen et al., 2008). To exclude precipitation outliers less than 0 and reduce the random errors, computations are only conducted on grid cells where and when there is at least one reporting observation, and both of the satellite-based precipitation products (i.e. IMERG\_Cal, IMERG\_Uncal and 3B42V7) and CPAP are above zero. The statistics (i.e. Bias, RMSE and CC) here are established from the daily precipitation rate, with an interval of 1 mm/day for mainland China and seven subregions.

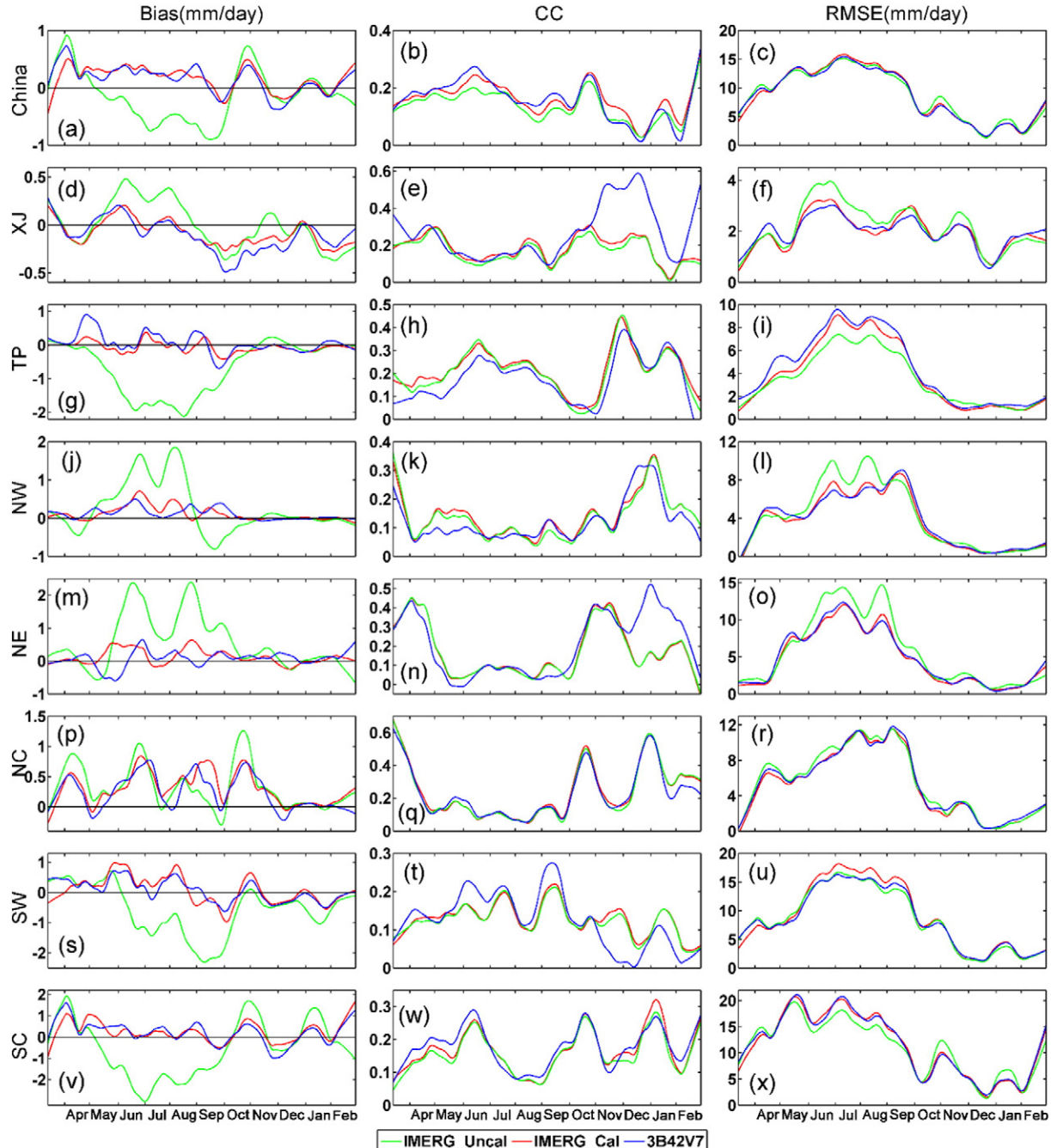


**Fig. 7.** Daily series of Bias, Correlation Coefficient (CC) and Root Mean Square Error (RMSE) between three satellite-based precipitation estimates and CPAP over China and seven subregions for (a–c) China, (d–f) XJ, (g–i) TP, (j–l) NW, (m–o) NE, (p–r) NC, (s–u) SW and (v–x) SC on 0.25° lat/lon grid box. Only the cells where there is at least one reporting gauge in CPAP and both satellite-based precipitation estimates and CPAP are above zero can be selected for computation.

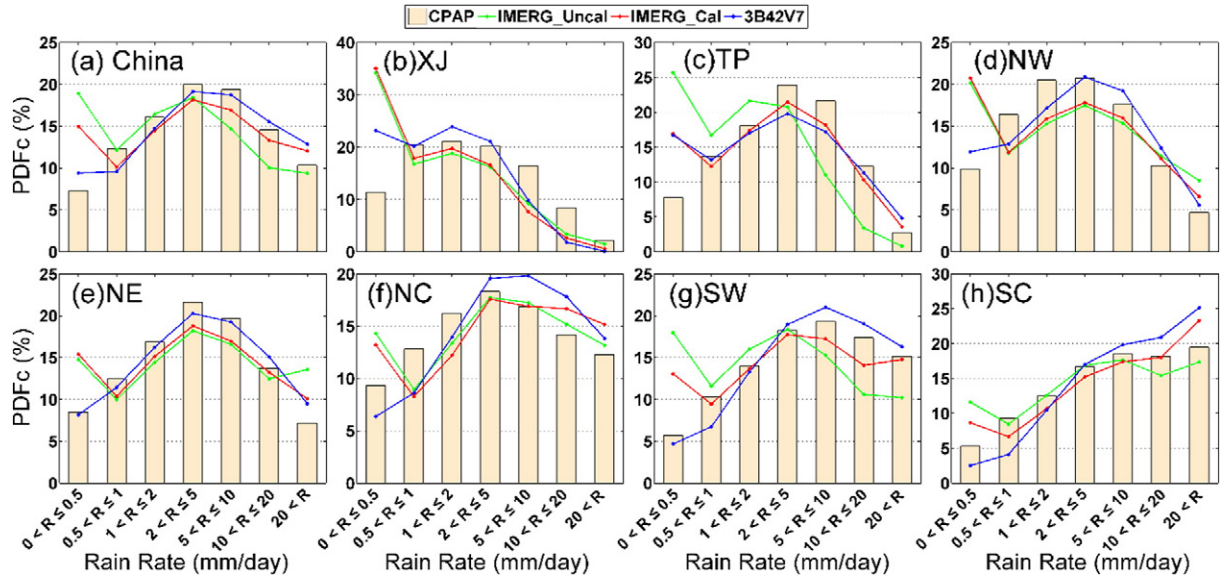


**Fig. 8.** Probability density function by occurrence (PDFc) of daily precipitation for cases with different intensities over China and seven subregions for (a) China, (b) XJ, (c) TP, (d) NW, (e) NE, (f) NC, (g) SW and (h) SC. Only grid cells where there is at least one reporting gauge and the IMERG precipitation estimates are non-zero can be selected for computing the PDFc.

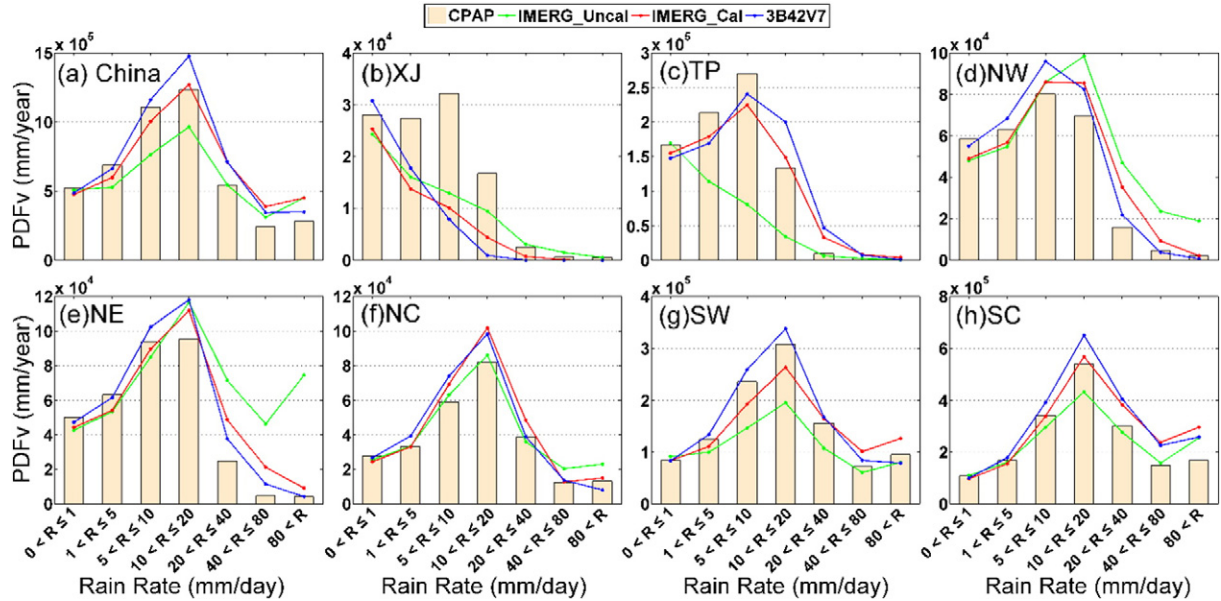


**Fig. 9.** Probability distribution functions by volume (PDFv) for cases with different intensities over China and seven subregions for (a) China, (b) XJ, (c) TP, (d) NW, (e) NE, (f) NC, (g) SW and (h) SC. Only cells where there is at least one reporting gauge and the IMERG precipitation estimates are non-zero can be selected for computing the PDFv.

As is shown in Fig. 7, the Bias of IMERG\_Uncal fluctuates greatly throughout the whole study period with significant negative values during the monsoon season from May to October over China. After bias correction, the Bias of IMERG\_Cal appears to be stable around the black zero line. 3B42V7 also shows the similar stable pattern. IMERG\_Cal and 3B42V7 give slightly high CC than IMERG\_Uncal and relatively higher CCs in summer than those in winter. The RMSE for the three products also displays a seasonally dependent variation with higher values during monsoon season and lower values during winter. This may be primarily a result of the greater rainfall volume in monsoon season. IMERG\_Uncal estimates much less precipitation over TP, SW, and SC but more precipitation over XJ, NW, and NE. This result is consistent with the analysis in Sections 3.1 and 3.2. The CCs of these three products are similar, yielding lower values in monsoon seasons over XJ, NW, NE and NC. The patterns of RMSEs for all three products over the various subregions are close over China.

### 3.4. Precipitation occurrence analysis

Accurate documentation of rainfall frequencies with different intensities is as important as that for the mean amount and spatiotemporal

**Table 1**

Thresholds of precipitation intensity ( $R$ ) for the probability distribution functions for occurrence (PDFc) and PDF by volume (PDFv).

Index	PDFc (mm/day)	PDFv (mm/day)
1	$0 < R \leq 0.5$	$0 < R \leq 1$
2	$0.5 < R \leq 1$	$1 < R \leq 5$
3	$1 < R \leq 2$	$5 < R \leq 10$
4	$2 < R \leq 5$	$10 < R \leq 20$
5	$5 < R \leq 10$	$20 < R \leq 40$
6	$10 < R \leq 20$	$40 < R \leq 80$
7	$R > 20$	$R > 80$

variation patterns of precipitation (Tian et al., 2007) since the same precipitation amount in the form of long-lasting light rain or a short-duration storm will yield quite different impacts in many aspects (Li et al., 2013; Shen et al., 2010b). Probability distribution functions (PDFs) can reveal the spatiotemporal inhomogeneity of precipitation and offer an insight into the dependence of estimate errors on precipitation rate and the potential effects from these errors on hydrological applications. In this section, the two IMERG products and 3B42V7 are examined against the reference dataset (CPAP) in capturing the occurrence of rainfall with different amounts throughout the whole study period. The PDFs by occurrence (PDFc) and the PDFs by volume (PDFv) as functions of the daily precipitation over mainland China and seven sub-regions are shown in Fig. 8 and Fig. 9, respectively. The thresholds of precipitation intensities ( $R$ ) for PDFc and PDFv are shown in Table 1.

When spatially interpolated from point observations, the reference data may lead to more events with reduced intensities because strong events tend to “spill” into adjacent grid boxes (Tian et al., 2007). In order to avoid the errors from interpolation, only data over grid boxes with at least one gauge report are included in the computation.

Both the IMERG products, as well as 3B42V7, overdetect light precipitation events (rain rate  $< 0.5 \text{ mm/day}$ ) over China, especially for XJ, TP, and NW (Fig. 8). This result may be related to the following aspects: First, the PMW-based algorithms used in IMERG are good at detecting heavy, convective precipitation events, but still tend to miss shallow and warm precipitation (Andermann et al., 2012; Shige et al., 2013). In addition, light precipitation is easily evaporated, partially or totally, in a dry environment (Chen et al., 2013b; Story et al., 2001; Surussavadee & Staelin, 2010; Tesfagiorgis et al., 2010), which leads to

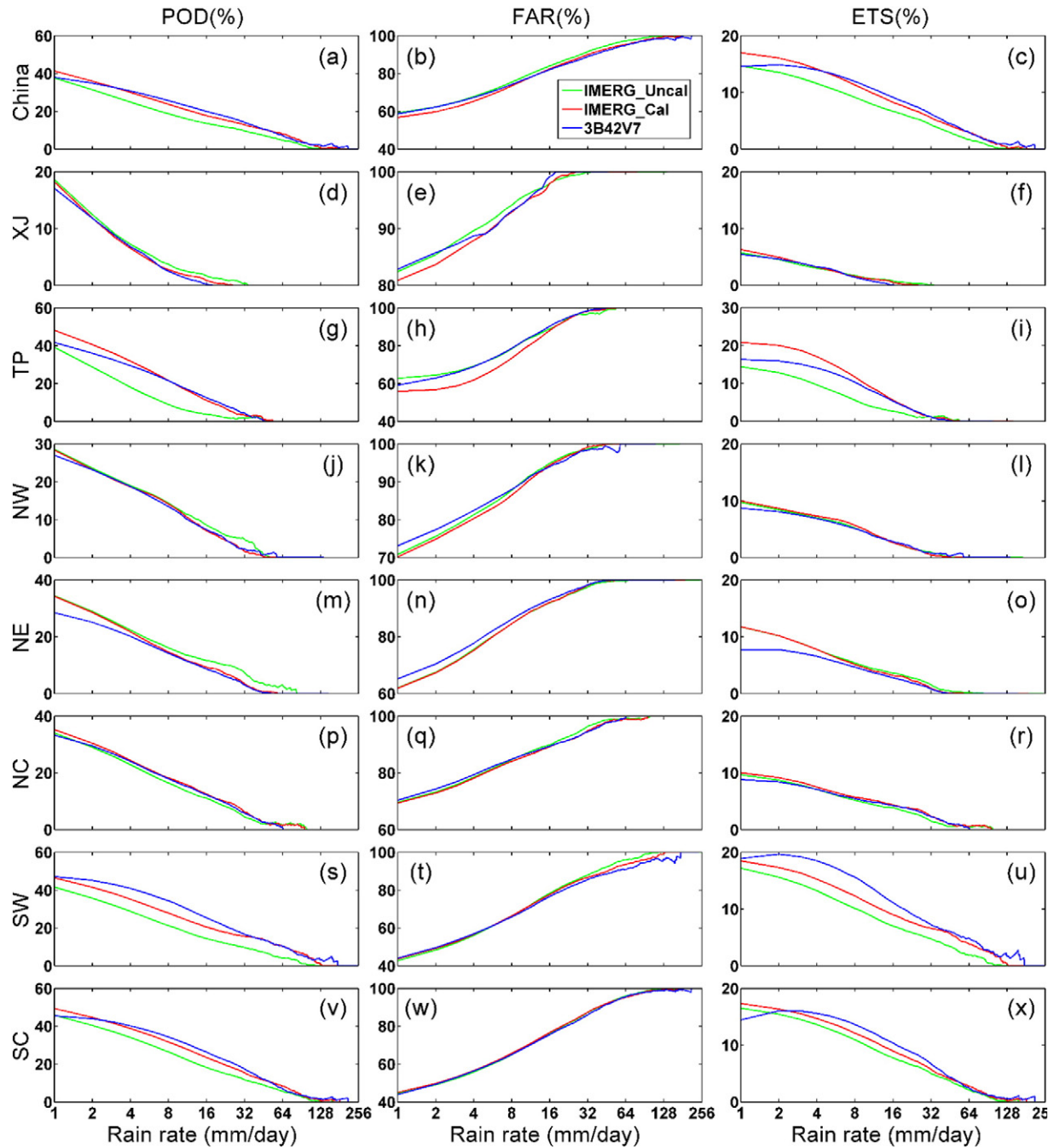


**Fig. 10.** Contingency metrics of Probability of Detection (POD), False Alarm Rate (FAR) and Equitable Threat Score (ETS) for precipitation in China and seven subregions for (a–c) China, (d–f) XJ, (g–i) TP, (j–l) NW, (m–o) NE, (p–r) NC, (s–u) SW and (v–x) SC. The log-scale is applied to improve the readability.

the overestimation of the frequency of light precipitation at the ground surface. When rain rate is more than 2 mm/day, IMERG\_Uncal seems to detect many less precipitating days over China, and a similar trend is found in SW and SC. Particularly, the underestimation over XJ is as large as 12% when the rain rate is in 5–10 mm/day. As expected, this underestimation is improved by the gauge-corrected IMERG\_Cal. 3B42V7 shows a relatively better performance in northwestern China (i.e. XJ and NW) but tends to underestimate rain rates less than 2 mm/day and overestimates rain rates more than 2 mm/day in NC, SW and SC.

As shown in Fig. 9, the IMERG products, in parallel with 3B42V7, slightly underestimate light rain volumes (<10 mm/day) and show overestimation in rain rate bins over 20 mm/day. Despite the great overdetection of the occurrence of precipitation when the rain rate is less than 2 mm/day, both the IMERG products demonstrate slight underdetection of precipitation volumes over XJ and NW, both of which are characterized by semi-arid and arid climates with strong evaporation (Fig. 9b and d). In XJ, all three products greatly underestimate precipitation volumes over 1 mm/day. This may result from several factors, including complicated terrain, strong evaporation processes, and sparse coverage of gauge stations. In addition, IMERG\_Uncal also demonstrates abnormal underestimation of precipitation volume over 1 mm/day in TP, which partially results from the underdetection of precipitation occurrence over 2 mm/day (Fig. 8c), although the gauge correction process in IMERG\_Cal distinctively improves such underestimation. Abnormal overestimation of heavy rain (>20 mm/day) for IMERG\_Uncal also can be seen in Fig. 9e, partially due to an excessive number of heavy rain events (Fig. 8e). This effect also provides a possible explanation for the overestimation of IMERG\_Uncal over NE, discussed in Section 3.1. In the typical monsoon areas (i.e. SW, SC and NC), the precipitation volume peaks at 10–20 mm/day. All three products yield similar distribution patterns, but different magnitudes of overestimation or underestimation. While IMERG\_Cal agrees with CPAP well when rain rates are less than 5 mm/day, it tends to detect more precipitation volume over 40 mm/day.

### 3.5. Contingency statistics

Probability of Detection (POD), False Alarm Ratio (FAR) and Equitable Threat Score (ETS) can help us to understand the nature of the occurrence errors (Ebert et al., 2007). The contingency statistics (POD, FAR and ETS) of the IMERG products and 3B42V7 as a function of daily precipitation rate are shown in Fig. 10. In general, both the IMERG products and 3B42V7 have low PODs (<50%) and ETSs (<25%), and high FARs (> 45%) over various regions, especially for the north part of China (e.g. XJ, TP, NW and NC). This performance is consistent with the result of precipitation occurrence shown in Fig. 8. The IMERG products and 3B42V7 have a similar performance. On the regional scale, the performances of all three products over SW and SC are better than other subregions, with relative higher PODs and ETSs and lower FARs. 3B42V7 shows a relatively poorer (better) performance over NE (SW) with lower (higher) POD and ETS. Interestingly, the bias-corrected IMERG\_Cal and 3B42V7 perform slightly poorer than IMERG\_Uncal according to the lower values of POD over XJ and NE, especially for the rain rate over 8 mm/day.

## 4. Summary and conclusion

IMERG algorithms incorporate a variety of precipitation observations from relevant satellite sensors (microwave and infrared) and ground-based gauge networks (GPCC gauge analysis) with half-hourly  $0.1^\circ \times 0.1^\circ$  resolution. Future developments of IMERG algorithms and utilization of IMERG datasets in operational applications rely on a more in-depth understanding of satellite errors and biases across different spatial and temporal scales. This paper provides an early and timely quantitative study of error characteristics for the final run post-research products of IMERG in the region of mainland China, including IMERG\_Uncal without

direct bias-correction and gauge-adjusted IMERG\_Cal. For comparison reference, 3B42V7 is evaluated in parallel with the IMERG products. The quantitative analysis is based on comparisons with the gauge-based reference dataset, CPAP, at multi-regions (China and its seven subregions) and at a range of temporal scales (from yearly mean to daily time series). In addition to the conventional statistical indices, frequency analysis and spatial analysis have also been included within this study. The main findings of this study are as follows:

- 1) For the one year precipitation analysis, IMERG\_Cal has a much better performance than IMERG\_Uncal with increased CC from 0.82 to 0.93, reduced RB from –7.15% to 1.12%, and RMSE from 0.87 mm/day to 0.56 mm/day over China. Compared with 3B42V7, IMERG\_Cal also shows a favorable performance in capturing the spatial patterns of precipitation with slightly lower RB (1.12% vs. 2.89%) over China during the whole study period. According to the Taylor diagrams in Fig. 4, IMERG\_Cal gives a relatively better performance than 3B42V7 in China, especially for NW and NE.
- 2) According to the seasonal analysis, all three products demonstrate poor performance in winter with the largest RB and smallest CC. IMERG\_Uncal performs poorest in terms of largest RB (–23.60%), RMSE (0.56 mm/day) and lowest CC (0.64), while IMERG\_Cal gives the highest CC (0.84) but relatively larger RB (–12.68%) compared to 3B42V7 (–9.07%).
- 3) IMERG\_Cal, IMERG\_Uncal, and 3B42V7 have low scores of POD (<50%) and ETS (<25%), and high scores of FAR (>45%) over China and seven subregions. IMERG\_Cal and 3B42V7 have the similar performance, with generally better scores than IMERG\_Uncal (Fig. 10).
- 4) IMERG\_Uncal significantly underestimates in SW, SC, and TP with RBs of –28.32%, –15.02% and –26.89%, respectively. It also demonstrates significant overestimation over NW, NE, and NC according to RBs (18.95%, 23.49% and 14.84%, respectively). IMERG\_Cal and 3B42V7 show a much better performance with reduced errors for these regions except for XJ where both the IMERG products overestimate the precipitation over desert regions in southern XJ.

The performance characteristics of IMERG\_Uncal and IMERG\_Cal, as well as 3B42V7, are identified and quantified over China in this study. Readers should keep in mind that there is a limitation to evaluate the characteristics of IMERG products due to the non-availability of long-term records. The performances of IMERG\_Cal and 3B42V7 are similar in terms of spatial precipitation patterns and corresponding statistics (i.e. RB, RMSE and CC). In addition, IMERG\_Uncal gives a relatively poorer performance than IMERG\_Cal and 3B42V7. When the IMERG products are used in semi-arid and arid areas, users should be careful for its overestimation of light rainfall events, which needs further investigation in the future.

## Acknowledgements

This work was supported in part by the National Natural Science Foundation of China (Grant No. 41371419, No. 91437214 and No. 41361022), the Special program for International Science & Technology Cooperation (2010DFA92720-04), One Thousand Youth Talents Plan of China (Xinjiang Project: 374231001) and the Hydrometeorology and Remote Sensing (HyDROS) Laboratory at The University of Oklahoma, OK, USA. The IMERG data were generated by the NASA/Goddard Space Flight Center's Mesoscale Atmospheric Processes Laboratory and PPS, which develop and compute IMERG as a contribution to GPM, and archived at the NASA PPS (<https://stompps.gsfc.nasa.gov/storm>). The TRMM-3B42V7 data were provided by the NASA/Goddard Space Flight Center's Laboratory for Atmospheres and freely obtained online ([ftp://disc2.nascom.nasa.gov/data/TRMM/Gridded/Derived\\_Products/3B42\\_V7/Daily/](ftp://disc2.nascom.nasa.gov/data/TRMM/Gridded/Derived_Products/3B42_V7/Daily/)). The reference dataset (CPAP) is provided by the National Meteorological Information Center (NMIC) and China Meteorological Administration (CMA) (<http://cdc.nmic.cn/sksj.do?method=ssrjscp>).

## Appendix A. Statistics over seven subregions

In this section, the statistics (RB, RMSE, FSE, and CC) between satellite-based precipitation estimates (IMERG\_Uncal, IMERG\_Cal and

3B42V7) and the reference dataset (CPAP) based on one year and seasonal precipitation over seven subregions are present in Table A1. The best performance for different time period over different subregions is highlighted with bold font.

**Table A1**

RB, RMSE, FSE and CC between different satellite-based products and CPAP based on one-year and seasonal precipitation over seven subregions.

Index	Time	Type	XJ	TP	NW	NE	NC	SW	SC
RB (%)	Year	IMERG_Uncal	−7.15	<b>−6.21</b>	−26.70	34.47	30.42	15.21	−28.34
		IMERG_Cal	<b>1.12</b>	−26.84	<b>0.15</b>	<b>7.39</b>	4.17	16.92	−6.39
		3B42V7	2.89	−31.55	7.83	8.69	<b>2.64</b>	<b>13.54</b>	<b>−0.46</b>
	Spring	IMERG_Uncal	<b>4.95</b>	<b>−11.82</b>	19.54	<b>14.25</b>	−8.78	38.11	<b>−1.74</b>
		IMERG_Cal	6.92	−24.19	<b>17.14</b>	15.36	<b>5.50</b>	26.21	−3.75
		3B42V7	10.54	−23.08	34.57	17.93	−13.03	<b>24.51</b>	7.26
	Summer	IMERG_Uncal	−13.41	16.86	−52.29	58.51	44.70	<b>5.05</b>	−30.34
		IMERG_Cal	<b>0.21</b>	<b>−16.37</b>	−6.11	<b>10.54</b>	<b>3.37</b>	9.28	−4.86
		3B42V7	2.62	−22.27	<b>1.27</b>	13.17	4.36	7.66	<b>0.21</b>
	Autumn	IMERG_Uncal	<b>−0.91</b>	<b>−6.93</b>	<b>−1.54</b>	15.69	56.32	14.17	−35.43
		IMERG_Cal	1.39	−30.21	2.73	5.18	17.50	19.78	−8.36
		3B42V7	−1.02	−51.61	4.57	<b>−0.02</b>	<b>9.91</b>	<b>15.92</b>	<b>−2.27</b>
RMSE mm/day	Winter	IMERG_Uncal	−23.60	−68.80	71.24	−57.79	−44.01	23.42	−53.30
		IMERG_Cal	−12.68	−55.09	<b>13.21</b>	−49.37	−32.27	33.81	−18.76
		3B42V7	<b>−9.07</b>	<b>−35.23</b>	18.90	−26.20	<b>15.39</b>	<b>4.70</b>	<b>−17.35</b>
	Year	IMERG_Uncal	0.87	0.38	0.71	0.51	0.63	0.51	1.87
		IMERG_Cal	0.56	0.33	<b>0.42</b>	<b>0.22</b>	<b>0.23</b>	0.39	1.33
		3B42V7	<b>0.52</b>	<b>0.31</b>	0.49	0.23	0.26	<b>0.35</b>	<b>1.10</b>
	Spring	IMERG_Uncal	1.08	0.68	0.68	0.38	0.53	1.06	2.00
		IMERG_Cal	<b>0.72</b>	0.55	<b>0.47</b>	<b>0.25</b>	<b>0.34</b>	0.68	1.46
		3B42V7	0.79	<b>0.51</b>	0.50	0.35	0.58	<b>0.66</b>	<b>1.34</b>
	Summer	IMERG_Uncal	2.30	0.83	1.93	1.51	1.96	1.45	4.78
		IMERG_Cal	1.42	0.64	<b>1.00</b>	0.62	0.70	<b>0.68</b>	3.57
		3B42V7	<b>1.30</b>	<b>0.56</b>	1.15	<b>0.57</b>	<b>0.69</b>	0.69	<b>2.91</b>
	Autumn	IMERG_Uncal	1.01	0.54	0.84	1.00	0.98	0.79	1.59
		IMERG_Cal	<b>0.55</b>	<b>0.48</b>	<b>0.48</b>	<b>0.36</b>	0.39	0.61	<b>0.88</b>
		3B42V7	0.56	0.53	0.51	<b>0.36</b>	<b>0.37</b>	<b>0.57</b>	0.90
	Winter	IMERG_Uncal	0.56	0.38	0.69	0.21	0.36	0.18	0.70
		IMERG_Cal	<b>0.36</b>	0.33	<b>0.43</b>	0.19	0.28	0.19	0.41
		3B42V7	0.37	<b>0.26</b>	0.47	<b>0.18</b>	<b>0.23</b>	<b>0.17</b>	<b>0.37</b>
FSE	Year	IMERG_Uncal	0.44	0.31	0.46	0.28	0.26	0.15	1.04
		IMERG_Cal	0.18	0.25	<b>0.16</b>	<b>0.05</b>	<b>0.04</b>	0.09	0.53
		3B42V7	<b>0.16</b>	<b>0.22</b>	0.22	0.06	0.05	<b>0.07</b>	<b>0.36</b>
	Spring	IMERG_Uncal	0.70	1.09	0.78	0.20	0.21	0.75	1.65
		IMERG_Cal	<b>0.32</b>	0.72	<b>0.38</b>	<b>0.09</b>	<b>0.09</b>	0.30	0.87
		3B42V7	0.37	<b>0.62</b>	0.42	0.17	0.25	<b>0.29</b>	<b>0.75</b>
	Summer	IMERG_Uncal	1.59	0.97	1.36	1.21	1.18	0.70	3.23
		IMERG_Cal	0.60	0.58	<b>0.36</b>	0.21	0.15	<b>0.15</b>	1.80
		3B42V7	<b>0.51</b>	<b>0.44</b>	0.48	<b>0.18</b>	<b>0.15</b>	0.16	<b>1.20</b>
	Autumn	IMERG_Uncal	0.70	0.59	0.81	1.02	0.84	0.29	0.82
		IMERG_Cal	<b>0.21</b>	<b>0.46</b>	<b>0.26</b>	<b>0.13</b>	0.13	0.17	<b>0.25</b>
		3B42V7	0.21	0.56	0.29	0.13	<b>0.12</b>	<b>0.16</b>	0.27
	Winter	IMERG_Uncal	0.62	0.49	2.38	0.28	0.33	0.12	0.58
		IMERG_Cal	<b>0.26</b>	0.37	<b>0.91</b>	0.26	0.19	0.14	0.19
		3B42V7	0.27	<b>0.24</b>	1.12	<b>0.23</b>	<b>0.13</b>	<b>0.12</b>	<b>0.16</b>
CC	Year	IMERG_Uncal	0.82	0.51	0.61	0.76	0.57	0.72	0.28
		IMERG_Cal	0.93	0.66	<b>0.86</b>	<b>0.91</b>	<b>0.79</b>	<b>0.93</b>	0.57
		3B42V7	<b>0.94</b>	<b>0.75</b>	0.82	<b>0.91</b>	0.73	0.92	<b>0.74</b>
	Spring	IMERG_Uncal	0.88	0.21	0.45	0.74	0.33	0.75	0.54
		IMERG_Cal	<b>0.95</b>	0.40	0.76	<b>0.89</b>	<b>0.66</b>	<b>0.88</b>	0.75
		3B42V7	<b>0.95</b>	<b>0.52</b>	<b>0.79</b>	0.84	0.32	0.87	<b>0.79</b>
	Summer	IMERG_Uncal	0.65	0.27	0.82	0.71	0.65	0.24	0.18
		IMERG_Cal	0.88	0.48	<b>0.87</b>	0.86	<b>0.74</b>	<b>0.85</b>	0.49
		3B42V7	<b>0.90</b>	<b>0.66</b>	0.83	<b>0.88</b>	0.73	0.83	<b>0.73</b>
	Autumn	IMERG_Uncal	0.70	0.51	0.30	0.31	0.42	0.69	0.72
		IMERG_Cal	<b>0.91</b>	<b>0.60</b>	<b>0.78</b>	0.85	<b>0.79</b>	<b>0.90</b>	<b>0.86</b>
		3B42V7	0.91	0.59	0.76	<b>0.87</b>	0.77	0.89	0.84
	Winter	IMERG_Uncal	0.64	0.17	0.41	0.16	0.08	0.85	0.56
		IMERG_Cal	<b>0.84</b>	0.44	<b>0.41</b>	0.23	0.24	<b>0.89</b>	0.82
		3B42V7	0.83	<b>0.66</b>	0.28	<b>0.25</b>	<b>0.59</b>	0.71	<b>0.86</b>

## References

- Adeyewa, Z.D., Nakamura, K., 2003. Validation of TRMM radar rainfall data over major climatic regions in Africa. *J. Appl. Meteorol.* 42, 331–347.
- Anagnostou, E.N., 2004. Overview of overland satellite rainfall estimation for hydro-meteorological applications. *Surv. Geophys.* 25, 511–537.
- Andermann, C., et al., 2012. Impact of transient groundwater storage on the discharge of Himalayan rivers. *Nat. Geosci.* 5, 127–132.
- Arkin, P.A., Xie, P., 1994. The Global Precipitation Climatology Project: first algorithm intercomparison project. *Bull. Am. Meteorol. Soc.* 75, 401–419.
- Bajracharya, S.R., et al., 2015. Systematic evaluation of satellite-based rainfall products over the Brahmaputra Basin for hydrological applications. *Adv. Meteorol.* 2015, 1–17.

- Barrera, D.F., Ceirano, E., Zucarelli, G.V., 2007. Differences in area-averaged rainfall depth over a mid-size basin from two remote sensing methods of estimating precipitation. Proceedings of Predictions in Ungauged Basins. PUB Kick-Off, Brasilia, IAHS Publ, IAHS Press, Wallingford, UK, pp. 121–128.
- Bothe, O., Fraedrich, K., Zhu, X.H., 2012. Precipitation climate of Central Asia and the large-scale atmospheric circulation. *Theor. Appl. Climatol.* 108, 345–354.
- Carr, L.E., Elsberry, R.L., 1995. Monsoonal interactions leading to sudden tropical cyclone track changes. *Mon. Wea. Rev.* 123, 265–289.
- Casas, C., et al., 2015. Potential of satellite rainfall products to predict Niger River flood events in Niamey. *Atmos. Res.* 163, 162–176.
- Chen, M.Y., et al., 2008. Assessing objective techniques for gauge-based analyses of global daily precipitation. *J. Geophys. Res.* 113, D04110.
- Chen, S., et al., 2013a. Evaluation and uncertainty estimation of NOAA/NSSL next-generation national mosaic quantitative precipitation estimation product (Q2) over the continental United States. *J. Hydrometeorol.* 14, 1308–1322.
- Chen, S., et al., 2013b. Similarity and difference of the two successive V6 and V7 TRMM multisatellite precipitation analysis performance over China. *J. Geophys. Res.* 118, 13060–13074.
- Chen, S., et al., 2013c. Evaluation of the successive V6 and V7 TRMM multisatellite precipitation analysis over the continental United States. *Water Resour. Res.* 49, 8174–8186.
- Chen, S., et al., 2014. Evaluation of high-resolution precipitation estimates from satellites during July 2012 Beijing flood event using dense rain gauge observations. *PLoS ONE* 9, e89681.
- Chen, Z., Qin, Y., Shen, Y., Zhang, S., 2016. Evaluation of Global Satellite Mapping of Precipitation Project daily precipitation estimates over the Chinese mainland. *Adv. Meteorol.* 2016, 1–15.
- Ciach, G.J., Krajewski, W.F., Villarini, G., 2007. Product-error-driven uncertainty model for probabilistic quantitative precipitation estimation with NEXRAD data. *J. Hydrometeorol.* 8, 1325–1347.
- Ebert, E.E., Janowiak, J.E., Kidd, C., 2007. Comparison of near-real-time precipitation estimates from satellite observations and numerical models. *Bull. Am. Meteorol. Soc.* 88, 47–64.
- Ferraro, R.R., Smith, E.A., Berg, W., Huffman, G.J., 1998. A screening methodology for passive microwave precipitation retrieval algorithms. *J. Atmos. Sci.* 55, 1583–1600.
- Gao, Y.C., Liu, M.F., 2013. Evaluation of high-resolution satellite precipitation products using rain gauge observations over the Tibetan Plateau. *Hydrol. Earth Syst. Sci.* 17, 837–849.
- Germann, U., Galli, G., Boscacci, M., Bolliger, M., 2006. Radar precipitation measurement in a mountainous region. *Q. J. R. Meteorol. Soc.* 132, 1669–1692.
- Ghajarnia, N., Liaghat, A., Arasteh, P.D., 2015. Comparison and evaluation of high resolution precipitation estimation products in Urmia Basin-Iran. *Atmos. Res.* 158, 50–65.
- Grody, N.C., 1991. Classification of snow cover and precipitation using the special sensor microwave imager. *J. Geophys. Res.* 96, 7423–7435.
- Guo, H., et al., 2015a. Comprehensive evaluation of high-resolution satellite-based precipitation products over China. *Atmospheric Chem. Phys.* 7, 1–25.
- Guo, H., et al., 2015b. Inter-comparison of high-resolution satellite precipitation products over Central Asia. *Remote Sens.* 7, 7181–7211.
- Habib, E., Haile, A.T., Tian, Y., Joyce, R.J., 2012. Evaluation of the high-resolution CMORPH satellite rainfall product using dense rain gauge observations and radar-based estimates. *J. Hydrometeorol.* 13, 1784–1798.
- Hong, Y., Hsu, K.L., Sorooshian, S., Gao, X.G., 2004. Precipitation estimation from remotely sensed imagery using an Artificial Neural Network Cloud Classification System. *J. Appl. Meteorol.* 43, 1834–1852.
- Hsu, K.-L., Sorooshian, S., 2008. Satellite-based precipitation measurement using PERSIANN system. In: Sorooshian, S., et al. (Eds.), *Hydrological Modelling and the Water Cycle*. Springer, Berlin Heidelberg, pp. 27–48.
- Hsu, K.L., Gao, X.G., Sorooshian, S., Gupta, H.V., 1997. Precipitation estimation from remotely sensed information using artificial neural networks. *J. Appl. Meteorol.* 36, 1176–1190.
- Huang, Y., et al., 2013. Evaluation of version-7 TRMM Multi-satellite Precipitation Analysis Product during the Beijing extreme heavy rainfall event of 21 July 2012. *Water* 6, 32–44.
- Huffman, G.J., et al., 2007. The TRMM multisatellite precipitation analysis (TMPA): quasi-global, multiyear, combined-sensor precipitation estimates at fine scales. *J. Hydrometeorol.* 8, 38–55.
- Huffman, G.J., et al., 2014. Algorithm Theoretical Basis Document (ATBD) version 4.4 for the NASA Global Precipitation Measurement (GPM) Integrated Multi-satellite Retrievals for GPM (IMERG). NASA 1–30 (Greenbelt).
- Joyce, R.J., Xie, P., 2011. Kalman filter-based CMORPH. *J. Hydrometeorol.* 12, 1547–1563.
- Joyce, R.J., Janowiak, J.E., Arkin, P.A., Xie, P.P., 2004. CMORPH: a method that produces global precipitation estimates from passive microwave and infrared data at high spatial and temporal resolution. *J. Hydrometeorol.* 5, 487–503.
- Karaseva, M.O., Prakash, S., Gairola, R.M., 2012. Validation of high-resolution TRMM-3B43 precipitation product using rain gauge measurements over Kyrgyzstan. *Theor. Appl. Climatol.* 108, 147–157.
- Kidd, C., et al., 2012. Intercomparison of high-resolution precipitation products over Northwest Europe. *J. Hydrometeorol.* 13, 67–83.
- Kubota, T., et al., 2007. Global precipitation map using satellite-borne microwave radiometers by the GSMA project: production and validation. *IEEE Trans. Geosci. Remote Sens.* 45, 2259–2275.
- Li, Z., Yang, D.W., Hong, Y., 2013. Multi-scale evaluation of high-resolution multi-sensor blended global precipitation products over the Yangtze River. *J. Hydrol.* 500, 157–169.
- Liu, M., et al., 2014. Evaluation of high-resolution satellite rainfall products using rain gauge data over complex terrain in southwest China. *Theor. Appl. Climatol.* 1–17.
- Liu, X.D., Wang, Y., 2011. Contrasting impacts of spring thermal conditions over Tibetan Plateau on late-spring to early-summer precipitation in southeast China. *Atmos. Sci. Lett.* 12, 309–315.
- Liu, Z., 2015. Comparison of versions 6 and 7 3-hourly TRMM Multi-satellite Precipitation Analysis (TMPA) research products. *Atmos. Res.* 163, 91–101.
- Lo Conti, F., Hsu, K.-L., Noto, L.V., Sorooshian, S., 2014. Evaluation and comparison of satellite precipitation estimates with reference to a local area in the Mediterranean Sea. *Atmos. Res.* 138, 189–204.
- Mei, Y.W., Anagnostou, E.N., Nikolopoulos, E.I., Borga, M., 2014. Error analysis of satellite precipitation products in mountainous basins. *J. Hydrometeorol.* 15, 1778–1793.
- Nurmi, P., 2003. Recommendations on the Verification of Local Weather Forecasts.
- Okamoto, K., Ushio, T., Iguchi, T., Takahashi, N., Iwanami, K., 2005. The global satellite mapping of precipitation (GSMAp) project. *Geoscience and Remote Sensing Symposium*, 2005. IGARSS 05. Proceedings 2005 IEEE International, pp. 3414–3416.
- Piccolo, F., Chirico, G.B., 2005. Sampling errors in rainfall measurements by weather radar. *Adv. Geosci.* 2, 151–155.
- Porcù, F., Milani, L., Petracca, M., 2014. On the uncertainties in validating satellite instantaneous rainfall estimates with raingauge operational network. *Atmos. Res.* 144, 73–81.
- Qian, W., Lin, X., 2005. Regional trends in recent precipitation indices in China. *Meteorog. Atmos. Phys.* 90, 193–207.
- Qin, Y., Chen, Z., Shen, Y., Zhang, S., Shi, R., 2014. Evaluation of satellite rainfall estimates over the Chinese mainland. *Remote Sens.* 6, 11649–11672.
- Schneebeli, M., Dawes, N., Lehning, M., Berne, A., 2013. High-resolution vertical profiles of X-band polarimetric radar observables during snowfall in the Swiss Alps. *J. Appl. Meteor. Climatol.* 52, 378–394.
- Seyyedi, H., Anagnostou, E.N., Beighley, E., McCollum, J., 2015. Hydrologic evaluation of satellite and reanalysis precipitation datasets over a mid-latitude basin. *Atmos. Res.* 164, 37–48.
- Sharif, H.O., Ogden, F.L., Krajewski, W.F., Xue, M., 2002. Numerical simulations of radar rainfall error propagation. *Water Resour. Res.* 38, 15–11–115–14.
- Shen, Y., Xiong, A., 2015. Validation and comparison of a new gauge-based precipitation analysis over mainland China. *Int. J. Climatol.* 36, 252–265.
- Shen, Y., Feng, M., Zhang, H., Gao, F., 2010a. Interpolation methods of China daily precipitation data. *J. Appl. Meteorol. Sci.* 21, 279–286.
- Shen, Y., Xiong, A.Y., Wang, Y., Xie, P.P., 2010b. Performance of high-resolution satellite precipitation products over China. *J. Geophys. Res.* 115, D02114.
- Shen, Y., et al., 2014. Uncertainty analysis of five satellite-based precipitation products and evaluation of three optimally merged multi-algorithm products over the Tibetan Plateau. *Int. J. Remote Sens.* 35, 6843–6858.
- Shige, S., Kida, S., Ashiwa, H., Kubota, T., Aonashi, K., 2013. Improvement of TMI rain retrievals in mountainous areas. *J. Appl. Meteor. Climatol.* 52, 242–254.
- Sorooshian, S., et al., 2000. Evaluation of PERSIANN system satellite-based estimates of tropical rainfall. *Bull. Am. Meteorol. Soc.* 81, 2035–2046.
- Sitzen, S., Sandholt, I., 2010. Evaluation of remote-sensing-based rainfall products through predictive capability in hydrological runoff modelling. *Hydrol. Process.* 24, 879–891.
- Story, G.J., Forecaster, H., Center, W.G.R.F., 2001. Determining WSR-88D Precipitation Algorithm Performance Using the Stage III Precipitation Processing System. 14. West Gulf River Forecast Center, Fort Worth, TX, pp. 1–699.
- Surussavadee, C., Staelin, D.H., 2010. Correcting microwave precipitation retrievals for near-surface evaporation. *Geoscience and Remote Sensing Symposium (IGARSS), 2010 IEEE International*, pp. 1312–1315.
- Tang, L., Tian, Y.D., Yan, F., Habib, E., 2015. An improved procedure for the validation of satellite-based precipitation estimates. *Atmos. Res.* 163, 61–73.
- Tang, Z.Y., Wang, Z.H., Zheng, C.Y., Fang, J.Y., 2006. Biodiversity in China's mountains. *Front. Ecol. Environ.* 4, 347–352.
- Taniguchi, A., et al., 2013. Improvement of high-resolution satellite rainfall product for typhoon Morakot (2009) over Taiwan. *J. Hydrometeorol.* 14, 1859–1871.
- Taylor, K.E., 2001. Summarizing multiple aspects of model performance in a single diagram. *J. Geophys. Res.* 106, 7183–7192.
- Tesfagiorgis, K., Mahani, S.E., Khanbilvardi, R., 2010. Bias correction of satellite rainfall estimation using a radar-gauge product. *Hydrol. Earth Syst. Sci.* 7, 8913–8945.
- Tian, Y., Peters-Lidard, C.D., Choudhury, B.J., Garcia, M., 2007. Multitemporal analysis of TRMM-based satellite precipitation products for land data assimilation applications. *J. Hydrometeorol.* 8, 1165–1183.
- Xie, P., Xiong, A.-Y., 2011. A conceptual model for constructing high-resolution gauge-satellite merged precipitation analyses. *J. Geophys. Res.* 116, D21106.
- Xie, P.P., Arkin, P.A., 1995. An intercomparison of gauge observations and satellite estimates of monthly precipitation. *J. Appl. Meteorol.* 34, 1143–1160.
- Xie, P.P., Arkin, P.A., 1996. Analyses of global monthly precipitation using gauge observations, satellite estimates, and numerical model predictions. *J. Clim.* 9, 840–858.
- Xie, P.P., et al., 2007. A gauge-based analysis of daily precipitation over East Asia. *J. Hydrometeorol.* 8, 607–626.
- Yin, Z.Y., Zhang, X.Q., Liu, X.D., Colella, M., Chen, X.L., 2008. An assessment of the biases of satellite rainfall estimates over the Tibetan Plateau and correction methods based on topographic analysis. *J. Hydrometeorol.* 9, 301–326.
- Zhou, T., Gong, D., Li, J., Li, B., 2009. Detecting and understanding the multi-decadal variability of the East Asian Summer Monsoon – recent progress and state of affairs. *Meteorologische Zeitschrift* 18, 455–467.
- Zhou, T.J., Yu, R.C., Chen, H.M., Dai, A., Pan, Y., 2008. Summer precipitation frequency, intensity, and diurnal cycle over China: a comparison of satellite data with rain gauge observations. *J. Clim.* 21, 3997–4010.